High-Order Conformal Symplectic FDTD Scheme

Wei Sha[1] and Xianliang Wu[2]
[1] Department of Electrical and Electronic Engineering, the University of Hong Kong, Pokfulam Road, Hong Kong
[2] Key Laboratory of Intelligent Computing & Signal Processing, Anhui University, Feixi Road 3, Hefei 230039, China
[1] wsha@eee.hku.hk

Introduction

The traditional finite-difference time-domain (FDTD) method [1], which is explicit second-order-accurate in both space and time, has been widely applied to electromagnetic computation and simulation. However, the FDTD method has two primary drawbacks. One is the inability to accurately model curved complex surfaces and material discontinuities by using the staircased approach with structured grids, and another is the significant accumulated errors from numerical dispersion and anisotropy. Hence fine grids are required to obtain accurate numerical results, which leads to vast memory requirements and high computational costs, especially for electrically-large domains and for long-term simulation.

For solving the first problem, a variety of conformal techniques have been proposed in [2-5]. For solving the second problem, high-order spatial methods [6-7] were developed, which can save computational resources by using coarse grids. However, how to model the curved surfaces with the high-order spatial methods is an open question. In other words, can we obtain the accurate numerical results under both curved boundary and coarse grid conditions?

In order to achieve the goal, the one-sided difference [6] was studied. However, the strategy ignored the shape of objects. Another method is the hybrid subgridding technique [7]. However, it must adopt spatial and temporal interpolation strategies to eliminate the spurious reflections between the coarse grids and the fine grids.

In this paper, a new high-order conformal symplectic FDTD(3,4) scheme is proposed to solve the electromagnetic scattering from three-dimensional curved perfectly conducting objects. The scheme can achieve the above goal without temporal and spatial interpolations.

Theory

For the electric field components, the update equations need not to be modified.

Figure 1

For the magnetic field components, the general Faraday's loops are shown in Fig .1. Using the trick in [8], the semi-discrete update equation for H_x field can be written as

978-1-4244-2642-3/08/$25.00 ©2008 IEEE

$$\frac{\partial}{\partial t}H_x(i,j+\frac{1}{2},k+\frac{1}{2},t)=\frac{9}{8}\times\frac{1}{\sqrt{\mu_0\varepsilon_0}\Delta S_1^*}$$
$$\times\{[\hat{E}_y(i,j+\frac{1}{2},k+1,t)l_{1,y}(i,j,k+1)-\hat{E}_y(i,j+\frac{1}{2},k,t)l_{1,y}(i,j,k)]$$
$$-[\hat{E}_z(i,j+1,k+\frac{1}{2},t)l_{1,z}(i,j+1,k)-\hat{E}_z(i,j,k+\frac{1}{2},t)l_{1,z}(i,j,k)]\} \quad (1)$$
$$-\frac{1}{24}\times\frac{1}{\sqrt{\mu_0\varepsilon_0}}\times[\frac{\hat{E}_y(i,j+\frac{1}{2},k+2,t)-\hat{E}_y(i,j+\frac{1}{2},k-1,t)}{\Delta_z}$$
$$-\frac{\hat{E}_z(i,j+2,k+\frac{1}{2},t)-\hat{E}_z(i,j-1,k+\frac{1}{2},t)}{\Delta_y}]$$

where Δ_y and Δ_z are, respectively, the lattice space steps in the y and z coordinate directions, ε_0 and μ_0 are the permittivity and the permeability of free space, $l_{1,y}$ and $l_{1,z}$ are the side lengths along the y and z directions outside the perfectly conducting object, and ΔS_1^* is the area of the modified inner loop L_1 outside the object.

To obtain the stable and accurate numerical results, we have

$$\Delta S_1^*=\begin{cases}\Delta S_1^*, \Delta S_1^*\geq\gamma\Delta S_1\\ \gamma\Delta S_1, \Delta S_1^*<\gamma\Delta S_1\end{cases} \quad (2)$$

where ΔS_1 is the constant area of the unmodified inner loop L_1, and γ is the threshold. The smaller γ results in better numerical precision but smaller time step to ensure the stability of the scheme.

Finally, the three-stage third-order symplectic integrators [9] are employed to discretize the time direction.

Due to the modification for the update equations of magnetic fields, the Courant-Friedrichs-Lewy (CFL) number will be decreased as

$$CFL^*=\frac{\lambda_T}{\sqrt{\lambda_S\cdot\lambda_s^*}},\ \lambda_S=2\sqrt{d}\times|\frac{1}{24}+\frac{9}{8}|,\ \lambda_s^*=\max_{\forall L_1}\{2\sqrt{d}\times|\frac{1}{24}+\frac{9}{8}\cdot\frac{\max_\nu(l_{1,\nu})\Delta_x}{\Delta S_1^*}|\} \quad (3)$$

where d is the space dimension, $\max_\nu(l_{1,\nu})$ is the maximum length of the four sides connected with the inner loop L_1, and λ_T is the temporal stability factor defined in [9]. The temporal stability factors are equal to 2 and 4.52 respectively for the second-order leap-frog method and the third-order symplectic integration scheme.

Numerical results

Without loss of generality, it is assumed that a plane wave of frequency 300MHz travels along the z direction, the electric field is polarized along the x direction, and the uniform space step is adopted. The threshold $\gamma=0.01$. For the high-order conformal symplectic FDTD(3,4) (HC-SFDTD(3,4)) scheme, the CFL number is about 0.45. For the low-order conformal FDTD(2,2) (LC-FDTD(2,2)) method, the CFL number is about 0.2.

The scattering from an electrically-small conducting circular cylinder of height 2m and radius 1m is considered. The symmetrical axis of the cylinder is placed along the y direction. Fig. 2 shows the relative two-norm errors of bistatic radar cross section (RCS) as a function of points per wavelength (PPW). It can be seen that the HC-SFDTD(3,4) scheme can obtain better numerical precision than the high-order staircased SFDTD(3,4) (HS-SFDTD(3,4)) approach and the LC-FDTD(2,2) method.

Figure 2

The next example considered is the scattering from an electrically-large conducting sphere of diameter 14m. In particular, we only use 7 PPW to model the curved surfaces. From Fig. 3, compared with the LC-FDTD(2,2) method and the HS-SFDTD(3,4) approach, the HC-SFDTD(3,4) scheme agrees with the Mie series solution very well. The relative two-norm errors of the bistatic RCS in H-plane for the LC-FDTD(2,2) method, the HS-SFDTD(3,4) approach, and the HC-SFDTD(3,4) scheme are, respectively, 7.3%, 12.1%, and 0.83%.

Figure 3

Within the same relative two-norm errors bound (1%), we change the settings of the space step and the CFL number, and the CPU time and memory consumed by different algorithms are recorded in Table I. From the table, the HC-SFDTD(3,4) scheme saves considerable memory and CPU time.

Table I

Conclusion

Using the locally conformal technique and the high-order symplectic integrators, the high-order conformal symplectic FDTD scheme is accurate and efficient for modeling the scattering from three-dimensional curved perfectly conducting objects. In addition, the decreased time step caused by the conformal model can be offset by using coarse grids.

References

[1] K. S. Yee, "Numerical solution of initial boundary value problems involving Maxwell's equations in isotropic media," IEEE Transactions on Antennas and Propagation, vol. 14, pp. 302-307, Mar 1966.

[2] T. G. Jurgens, A. Taflove, K. Umashankar, and T. G. Moore, "Finite-difference time-domain modeling of curved surfaces," IEEE Transactions on Antennas and Propagation, vol. 40, pp. 357-366, Apr 1992.

[3] S. Dey and R. Mittra, "A locally conformal finite-difference time-domain algorithm for modeling three-dimensional perfectly conducting objects," IEEE Microwave and Guided Wave Letters, vol. 7, pp. 273-275, Sep 1997.

[4] W. H. Yu and R. Mittra, "A conformal FDTD algorithm for modeling perfectly conducting objects with curve-shaped surfaces and edges," Microwave and Optical Technology Letters, vol. 27, pp. 136-138, Oct 2000.

[5] T. Xiao and Q. H. Liu, "Enlarged cells for the conformal FDTD method to avoid the time step reduction," IEEE Microwave and Wireless Components Letters, vol. 14, pp. 551-553, Dec 2004.

[6] A. Yefet and P. G. Petropoulos, "A staggered fourth-order accurate explicit finite difference scheme for the time-domain Maxwell's equations," Journal of Computational Physics, vol. 168, pp. 286-315, Apr 2001.

[7] S. V. Georgakopoulos, C. R. Birtcher, C. A. Balanis, and R. A. Renaut, "HIRF penetration and PED coupling analysis for scaled fuselage models using a hybrid subgrid FDTD(2,2)/FDTD(2,4) method," IEEE Transactions on Electromagnetic Compatibility, vol. 45, pp. 293-305, 2003.

[8] W. Sha, X. L. Wu, Z. X. Huang, and M. S. Chen, "A new conformal FDTD(2,4) scheme for modeling three-dimensional curved perfectly conducting objects," IEEE Microwave and Wireless Components Letters, vol. 18, pp. 149-151, Mar 2008.

[9] W. Sha, Z. X. Huang, M. S. Chen, and X. L. Wu, "Survey on symplectic finite-difference time-domain schemes for Maxwell's equations," IEEE Transactions on Antennas and Propagation, vol. 56, pp. 493-500, Feb 2008

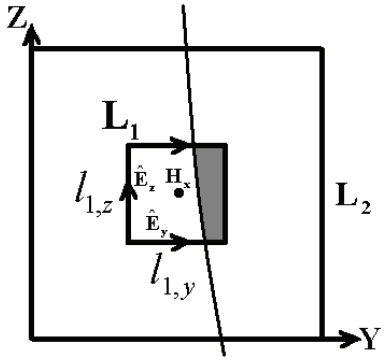

Fig. 1. The general Faraday's loops for the fourth-order staggered difference. The dot denotes H_x field. The four electric field components near from H_x link the inner loop L_1, and those far from H_x link the outer loop L_2. $l_{1,y}$ and $l_{1,z}$ are the side lengths along the y and z directions outside the perfectly conducting object. The gray region denotes the region inside the object.

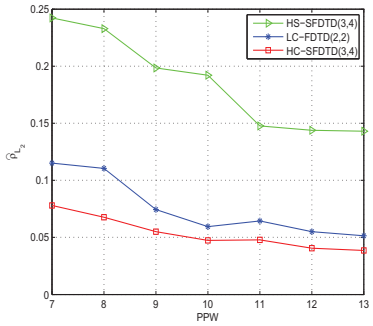

Fig. 2. The relative two-norm errors of the bistatic RCS in E-plane.

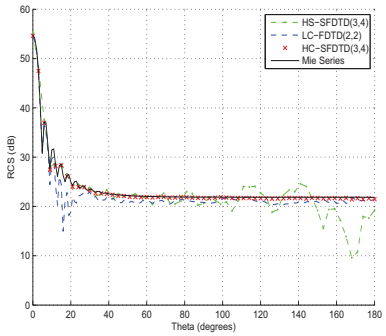

Fig. 3. The bistatic RCS in H-plane.

TABLE I The consumed CPU time and memory under the same relative two-norm errors condition.

Strategy	PPW	CFL	Time (s)	Memory (MB)
HC-SFDTD(3,4)	7	0.50	5891	258
HS-SFDTD(3,4)	16	1.00	56279	1318
LC-FDTD(2,2)	13	0.20	23359	820